UC Irvine

Title

Origin of tropospheric ozone at remote high northern latitudes in summer

Permalink

https://escholarship.org/uc/item/5531x9z9

Journal

Journal of Geophysical Research, 101(D2)

ISSN

0148-0227

Authors

Mauzerall, DL
Jacob, DJ
Fan, S-M
et al.

Publication Date

1996-02-20

DOI

10.1029/95jd03224

Copyright Information

Peer reviewed

Origin of tropospheric ozone at remote high northern latitudes in summer

D.L. Mauzerall[1], D.J. Jacob[1], S.-M. Fan[1,2], J.D. Bradshaw[3], G.L. Gregory[4], G.W. Sachse[4], and D.R. Blake[5]

Abstract. We quantify the tropospheric ozone budget over remote high northern latitudes in summer using chemical and meteorological measurements between 0 and 6-km made during the summer of 1990 Arctic Boundary Layer Expedition (ABLE 3B). We include all components of the ozone budget, both sinks (in situ photochemical loss and deposition); and sources (in situ photochemical production, advection of pollution ozone into the region, production in biomass wildfire plumes, and downwards transport from the upper troposphere/stratosphere). In situ production and loss of ozone are calculated with a photochemical model. The net influx of pollution ozone from North America and Eurasia is estimated from the average enhancement ratio of $\Delta O_3/\Delta C_2Cl_4$ observed in pollution plumes and scaled by the net influx of C_2Cl_4. The contribution of ozone produced in biomass wildfire plumes is estimated from the average enhancement ratio of $\Delta O3/\Delta CO$ in aged fire plumes. Regional photochemical production and loss in the 0-6 km column are found to be approximately equal; hence, net photochemical production is near zero. However, when ozone production and loss terms are separated, we find that dispersed in situ photochemical production driven by background NO levels (5-10 pptv) is the largest source term in the ozone budget (62%). Influx of stratospheric ozone is of secondary importance (27%), long-range transport of pollution ozone makes a small contribution (9%), and photochemical production of ozone within biomass wildfire plumes is a relatively negligible term (2%) in the budget. Biomass fires and transport of anthropogenic pollution into the region may however have a major effect on the ozone budget through enhancement of background NO_x mixing ratios which increase dispersed photochemical production. Using a 1-D time-dependent photochemical model between 0 and 6 km, we obtain good agreement between the observed and model-generated vertical ozone profiles. We find that in situ photochemistry within the 0-6 km column accounts for nearly 90% of the ozone mixing ratio within the boundary layer, while above 5 km it accounts for only about 40%. Although photochemical production of ozone within the 0-6 km column is larger than the other source terms combined, the 1-D model results indicate that influx from above is necessary to account for the observed increase in ozone mixing ratios with altitude.

1. Introduction

Ozone concentrations in industrialized regions of the northern hemisphere in summer have increased substantial-

[1]Department of Earth and Planetary Sciences and Division of Applied Science, Harvard University, Cambridge, Massachusetts.

[2] Now at Department of Geology and Geophysical Sciences, Princeton University, Princeton, New Jersey.

[3]School of Earth and Atmospheric Science, Georgia Institute of Technology, Atlanta, Georgia.

[4] NASA Langley Research Center, Hampton, Virginia.

[5]Department of Chemistry, University of California at Irvine, Irvine, California.

ly in the past century [*Logan*, 1985; *Intergovernmental Panel on Climate Change*, 1990; *Staehelin et al.*, 1994]; however, the global extent of human influence on tropospheric ozone remains unclear. A better understanding of the relative magnitude of sources of tropospheric ozone is crucial because ozone plays a central role in regulating the oxidizing capacity and hence the chemical composition of the lower atmosphere. Photolysis of ozone produces $O(^1D)$, which then reacts with water vapor to form the hydroxyl radical (OH). The hydroxyl radical is the primary oxidant for the removal of a variety of atmospheric pollutants and greenhouse gases, including CO, CH_4, other nonmethane hydrocarbons (NMHCs), and hydrohalocarbons (HCFCs). Ozone itself absorbs infrared radiation and is a greenhouse gas in the upper troposphere [*Lacis et al.*, 1990]. In addition, ozone is an oxidant which has detrimental effects on vegetation and human health. For all the above reasons, it is critical to understand what controls the ozone budget and how human activities may perturb it.

The distribution of tropospheric ozone is determined by a complex interplay of chemical and dynamical processes. Ozone enters the troposphere from the stratosphere, is advected from one region of the troposphere to another, and is produced within the troposphere by photochemical oxidation of CO and hydrocarbons in the presence of nitrogen oxides ($NO_x = NO + NO_2$). Ozone is lost via photolysis, reactions with radicals, and deposition to the Earth's surface. The lifetime of ozone in the troposphere varies from days to months, and hence ozone concentrations vary with latitude, altitude and season [Logan, 1985].

There is a long-standing debate regarding the relative importance of stratospheric and photochemical sources of ozone in the troposphere. Levy et al. [1985] summarized the literature supporting the view that tropospheric ozone concentrations are primarily controlled by transport from the stratosphere and surface destruction. Calculations conducted by Levy et al. [1985] using a general circulation/transport model without chemistry found that their simulation of tropospheric ozone was in general agreement with observations. They did, however, report evidence for significant production in the troposphere at latitudes north of 40°N. Other authors have supported the view that the dominant source of tropospheric ozone is photochemical rather than stratospheric, at least on the scale of the northern hemisphere [Fishman et al., 1979; Liu et al., 1980; Chameides and Tan, 1981; Logan et al., 1981; Liu et al., 1987]. This early work, however, was hampered by the paucity of data for NO_x, the limiting precursor for ozone formation in the troposphere. A large number of measurements of NO_x mixing ratios have recently been compiled from various regions of the world [Carroll & Thompson, 1995]. Photochemical model studies based on these measurements indicate that ozone production in the remote troposphere is sufficiently large to cancel chemical loss, resulting in either a small net production or a small net loss of ozone [Chameides et al., 1989; Chameides et al., 1990; Jacob et al., 1992a; Liu et al., 1992].

We present here an analysis of the summertime sources and sinks of tropospheric ozone in remote high northern latitudes. Our analysis uses chemical and meteorological data collected during the summer of 1990 from aircraft flights over Subarctic eastern Canada as part of the Arctic Boundary Layer Expedition 3B (ABLE 3B). This region is of particular interest because transport from the stratosphere to the troposphere is particularly strong at high northern latitudes [Danielsen, 1968; Shapiro, 1980; Shapiro et al., 1987], and because the region is downwind of polluted continents and therefore receives an influx of anthropogenic O_3 and NO_x [Jacob et al., 1993; Bakwin et al., 1994]. Extensive biomass wildfires, which supply an additional source of NO_x [Singh et al., 1994; Sandholm et al., 1994; Talbot et al., 1994], also take place in the region during the summer [Stocks, 1991]. Hence conditions may exist for both highly efficient photochemical production of ozone and a strong stratospheric influx.

Previous analyses of the ABLE 3B data concluded that ozone distributions over Subarctic eastern Canada are im-

pacted by long-range transport of urban pollution, forest fire emissions, sporadic encounters with tropical air and influx from the stratosphere [Anderson et al., 1994; Browell et al., 1994; Talbot et al., 1994]. These influences have clear signatures and are hence directly detectable in the data. Dispersed in situ photochemical production of ozone within the high northern latitude troposphere driven by background NO_x levels may also be important but is harder to detect. Our inclusion of a modeling component permits a quantification of this source. As shown below, we find that dispersed in situ photochemical production provides the dominant source of tropospheric ozone in the ABLE 3B region and, we argue, more generally at high northern latitudes in summer. We find influx of stratospheric ozone to be of secondary importance, long-range transport of pollution ozone to make a small contribution, and photochemical production of ozone within biomass wildfire plumes to be a relatively negligible term in the budget.

This paper is divided into five sections. Section 2 provides an overview of the observations used in the analysis. Section 3 describes the approach used to evaluate the budget of tropospheric ozone north of 45°N on the basis of the ABLE 3B measurements. Section 3 independently quantifies the different ozone sources (in situ photochemical production, influx of midlatitude pollution, local production within biomass wildfire plumes, and influx from the upper troposphere/stratosphere) and ozone sinks (in situ photochemical loss and deposition). Section 4 is a discussion of results including the derived ozone budget and an illustrative one-dimensional (1-D) model assessment, and section 5 is a summary of the analysis.

2. Observations

The ABLE 3B made chemical and meteorological measurements during aircraft flights over eastern Canada (45°-63°N latitude, 50° - 106° W longitude, and 0-6 km altitude) during July and August 1990 [Harriss et al., 1994a]. Figure 1 is a map of the experimental region. Species measured aboard the aircraft included O_3, NO, NO_2, total reactive odd-nitrogen (NO_y), peroxyacetyl nitrate (PAN), CO, CO_2, nonmethane hydrocarbons (NMHCs), UV radiation, H_2O, and several chlorinated compounds of exclusively industrial origin including C_2Cl_4, CH_3CCl_3, and CFC-11. Our analysis of biomass wildfire and pollution plumes uses the archived data from all flights shown in Figure 1, including transit flights over the northeastern United States. Our photochemical calculations use a merged data base of 579 points collected entirely within eastern Canada (missions 2-20) that was created by averaging the concentration of measured species over the 90 second intervals for which NO measurements were available. Measurements cover from 0800-1900 local solar time (defined as maximum solar elevation at noon).
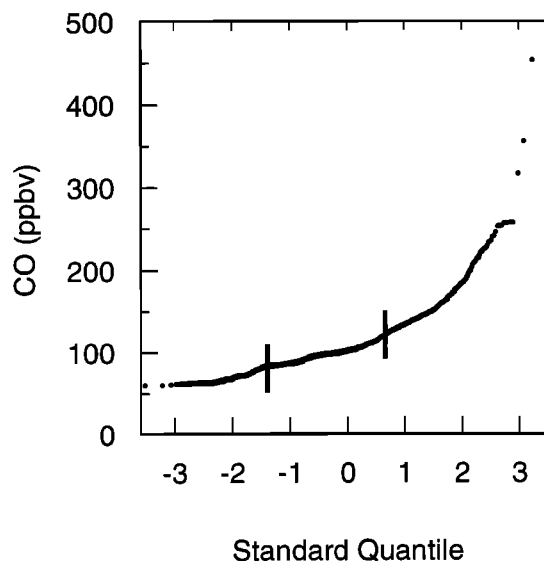
One objective of the ABLE 3B expedition was to characterize the composition of biomass wildfire and pollution plumes. Hence the database is biased towards more polluted air [Harriss et al., 1994b; Browell et al., 1994]. To remove

ABLE-3B Flight Paths
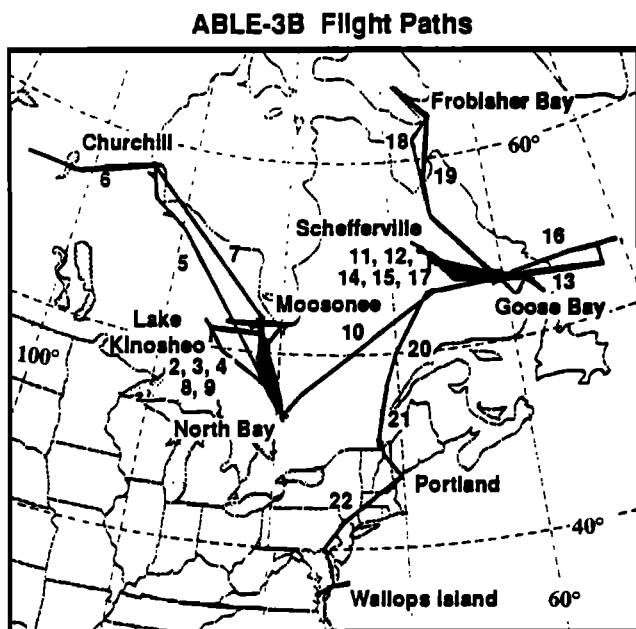
Figure 1. Map of Arctic Boundary Layer Expedition (ABLE 3B) aircraft flight paths used in analysis. Numbers on the map identify individual flights. Adapted from *Shipham et al.* [1994].

Standard Quantile

Figure 2a. Probability distribution function of CO concentrations in ABLE 3B plotted against the normal (Gaussian) distribution. The x-axis gives quantiles of standard normal such that ±1 represents ±1σ. A population of points with a normal distribution appears as a straight line. CO concentrations between 80 and 110 ppbv (vertical bars) are taken as representative of the regional atmospheric background.

this bias and define a representative background for the regional atmosphere, we compare the probability distribution function (pdf) of CO mixing ratios from the merged database to a Gaussian distribution (Figure 2a). We define the regional background as the approximately normal population represented by CO levels between 80 and 110 ppbv (299 points) which thus excludes encounters with tropical air as well as pollution and biomass wildfire plumes. Our definition of the regional background is consistent with long-term measurements of CO at Barrow, Alaska, which indicate a mean concentration of 97 ± 9 ppbv for July - August 1990 (P. Novelli, personal communication, 1995). Figure 2b shows the pdf of NO concentrations for the entire database and for the data subset defined as background air. Our definition of background air effectively excludes high-NO_x plumes.

To characterize the regional composition of the troposphere, mean mixing ratio versus altitude profiles for O_3, CO, NO, C_2H_4, C_2H_6, C_3H_8, isoprene, and C_2Cl_4 are shown in Figure 3. To compensate for uneven sampling throughout the day of species with a diurnal variation in concentration, we obtained these profiles by binning the data into 1-km altitude bins and then dividing the data within each altitude bin into 2-hour time intervals symmetrically around 12 noon. Morning/evening folding was used to compensate for a lack of early morning measurements. The means of each 2-hour time interval within each 1-km altitude bin were averaged to yield the profile of a given species with altitude. For O_3, CO, NO, and C_2Cl_4 two profiles are presented; the first (dashed line) includes all the data, the second (solid line) includes only the regional background air. For the NMHCs, only data from background air are shown.

Similar chemical and meteorological measurements to ABLE 3B were made during ABLE 3A in the summer of 1988 over Alaska [*Harriss et al.*, 1992]; however, ABLE 3A was not attempting to characterize biomass burning or pollution plumes. The chemical composition of the ABLE 3A region is similar to the background air in ABLE 3B as defined here. This similarity suggests that background air in the Arctic troposphere in summer has a relatively homoge-

Standard Quantile
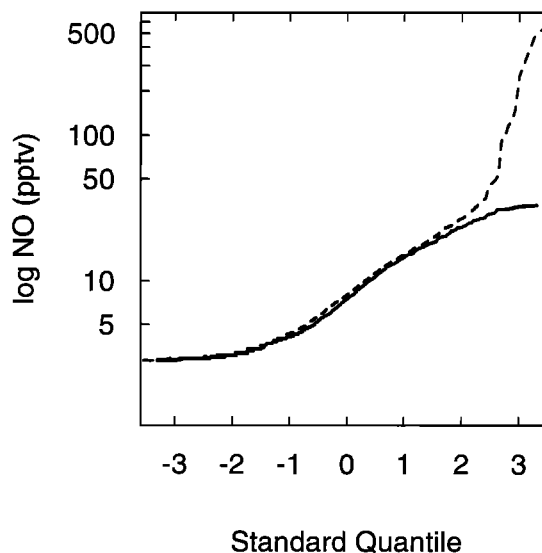
Figure 2b. Probability distribution function of NO concentrations for the entire ABLE 3B merged data set (dashed line) and for the data subset representative of the regional background as defined by 80<CO<110 ppbv (solid line).
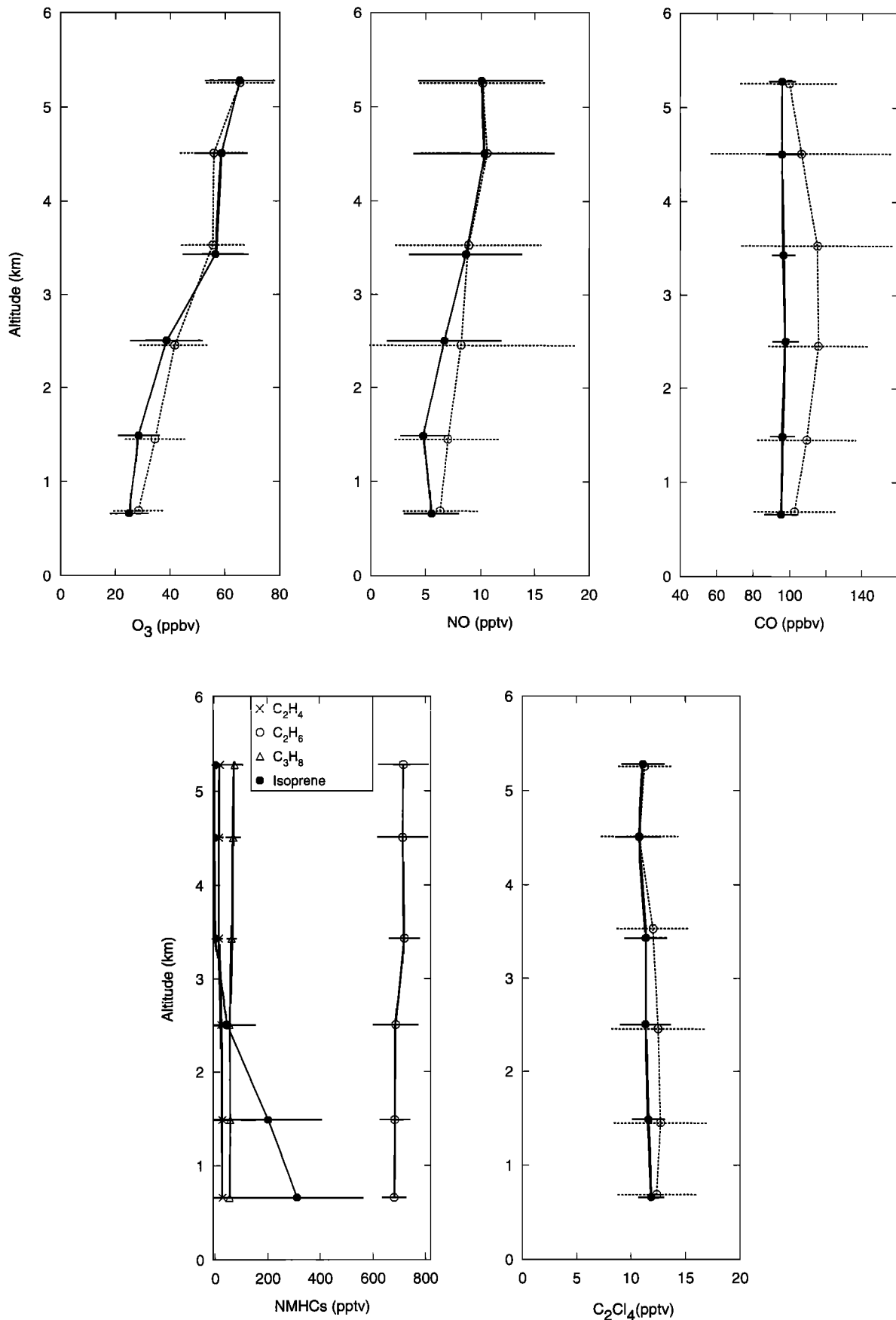
Figure 3. Mean daytime (4-20 solar time) mixing ratio profiles in ABLE 3B merged data set. Dashed lines include all data, solid lines include only the data subset with 80<CO<110 ppbv which defines regional background air. Horizontal bars indicate one standard deviation from the mean.

neous composition due in part to the jet stream which isolates it from the more polluted midlatitudes [*Barrie*, 1986].

3. Regional Ozone Budget

We focus our analysis on a "remote high northern latitudes" region defined as the circumpolar cap north of 45°N, excluding industrial areas of northern Europe, and extending from the surface to 6-km altitude (ceiling of the ABLE 3B aircraft). The size of this domain was chosen to accommodate the relatively long lifetime of ozone (averaging 26 days, as discussed in section 4). The regional ozone budget we calculate separates ozone sources (in situ photochemical production, advection of pollution ozone from midlatitude continents, local production within biomass wildfire plumes, and influx from the upper troposphere/stratosphere) from ozone sinks (in situ photochemical loss and deposition). Figure 4 is a schematic of the ozone source and sink terms contributing to the budget. Quantitative estimates for each of these terms are presented below.

Photochemistry

The effect of regional photochemistry on ozone is defined by the production and loss rates of the odd oxygen (O_x) family ($O_x \equiv O_3 + O(^1D) + O(^3P) + NO_2 + 2NO_3 + 3N_2O_5 + $ PAN). This definition accounts for the rapid cycling between ozone and other forms of O_x. PAN is included in this definition of O_x to account for the rapid cycling of PAN and NO_2 at the warm temperatures of the lower troposphere in summer.

The only significant source of O_x is by reaction (1):

(R1) $RO_2 + NO \rightarrow RO + NO_2$

where RO_2 represents the ensemble of peroxy radicals produced by oxidation of CO and hydrocarbons. Loss of O_x is primarily by reactions (2)-(4):

(R2) $O(^1D) + H_2O \rightarrow 2OH$

(R3) $O_3 + OH \rightarrow HO_2 + O_2$

(R4) $O_3 + HO_2 \rightarrow OH + 2O_2$
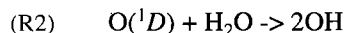
plus a minor sink from ozonolysis of olefins including isoprene.

Rawinsonde measurements made at the ABLE 3B surface site at Schefferville, Quebec (Figure 1), indicate a typical afternoon mixed layer depth of 2.25 km [*Fitzjarrald and Moore*, 1994] which is used in what follows to partition the boundary layer from the free troposphere. We calculate O_x production and loss rates in the free troposphere using a zero-dimensional (0-D) instantaneous steady state (ISS) photochemical model applied to each regional background point in the merged ABLE 3B data set. For each point the 0-D model uses as constraints the UV radiation flux measured by zenith and nadir Eppley radiometers, the observed temperature, dew point, altitude, and mixing ratios of O_3, CO, NO, C_{1-7} alkanes, C_{2-3} alkenes, isoprene, benzene, toluene and acetone. It then solves the local chemical instantaneous steady state equations for radicals other than NO, as well as for aldehydes, peroxides, ketones, HNO_2, and HNO_4. The NO_2 measurement aboard the aircraft may have suffered from positive interference [*Crawford et al.*, 1995] and we choose therefore to compute NO_2 concentrations from the model. A comparison of measured versus modeled NO_2 concentrations in ABLE 3B is given by *Fan et al.* [1994].

The photochemical mechanism is based on recent compilations of kinetic and product data [*Atkinson*, 1990; *Atkinson*
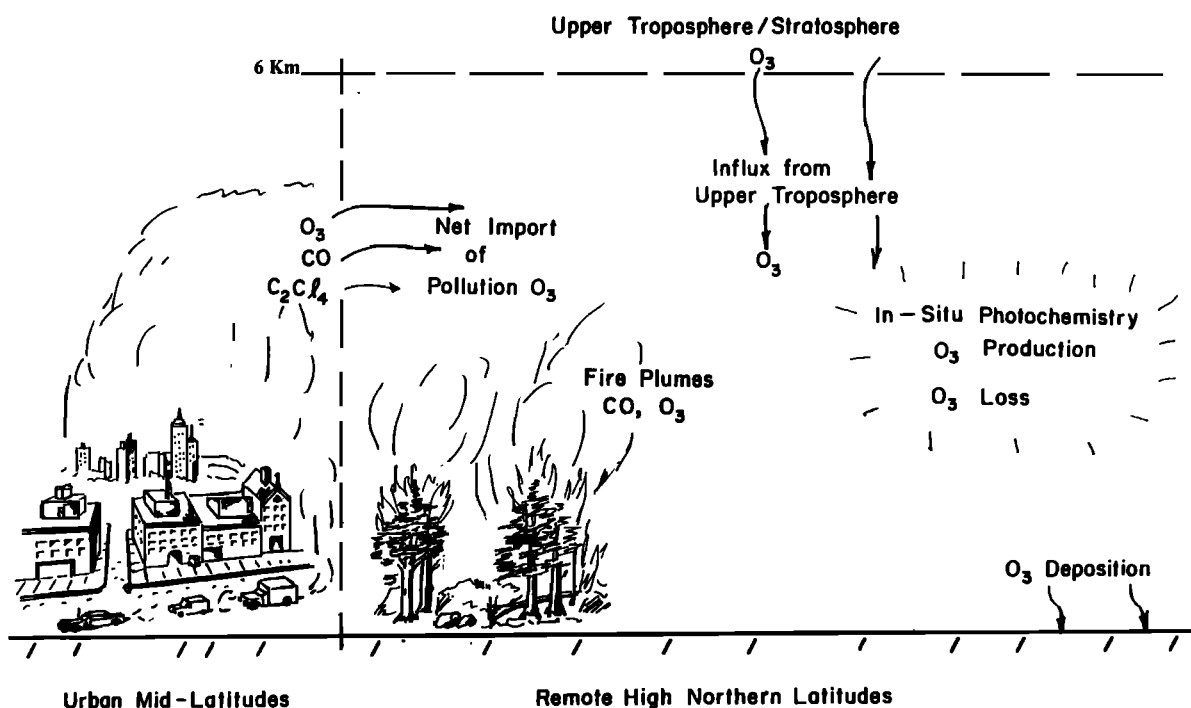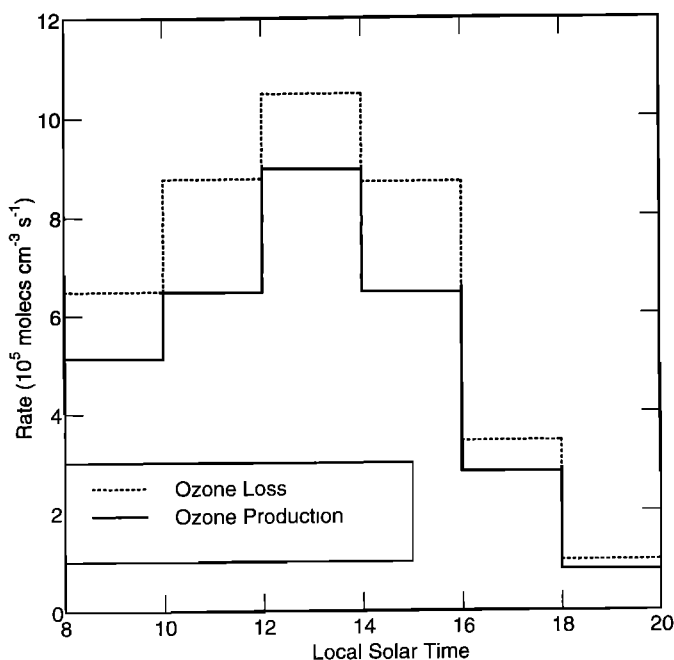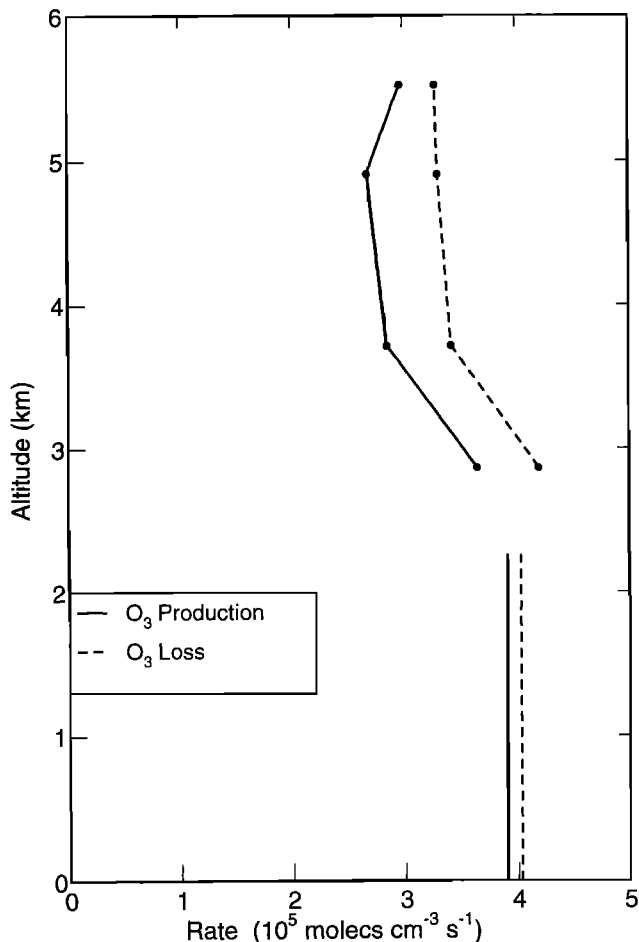

Figure 4. Schematic of the ozone budget for 0-6 km column at remote high northern latitudes.

et al., 1992; *DeMore et al.*, 1992; *Tuazon and Atkinson*, 1989, 1990a,b]. The NO_2 photolysis rate coefficient, J_{NO2}, is obtained from the Eppley UV fluxes with the parameterization of *Chameides et al.* [1990]. Photolysis rate coefficients for other species are calculated using a six-stream radiative transfer code for the clear-sky, Rayleigh scattering atmosphere with zero surface albedo [*Logan et al.*, 1981], and are then scaled by the ratio of J_{NO2} derived from the UV measurements to J_{NO2} calculated with the code (the mean and standard deviation of J_{NO2} (measured) / J_{NO2} (calculated) = 1.1±0.3). The overhead ozone column used in the radiation calculation is obtained from daily Total Ozone Mapping Spectrometer (TOMS) satellite measurements on an approximately 1° × 1° scale, and ranges from 290 to 360 Dobson units.

Greater accuracy in the photochemical model computation could be obtained by using a diel steady state (DSS) approach, where chemical steady state for a species is defined by the repeatability of the diel cycle in a time-dependent calculation. In a comparison of ISS and DSS approaches for computing ozone production in a point model, *D. J. Jacob et al.* (The origin of ozone and NO_x in the tropical troposphere: a photochemical analysis of aircraft observations over the South Atlantic basin, submitted to *Journal of Geophysical Research*, 1995) found agreement to within 10% between the two approaches for 0800-1600 local solar time (ST). However, the ISS calculation underestimated ozone production at lower sun angles. In our data set, since nearly 75% of the daily total ozone production occurred between 0800 and 1600 ST as is indicated in Figure 5, underestimation of ozone production should be small.

Figure 6. The 24-hour average ozone production and loss profiles (solid and dashed lines, respectively) computed for regional background air (80<CO<110 ppbv).

Figure 5. Diurnal cycle of ozone production and loss computed for background air (80<CO<110 ppbv) in the free troposphere (2.25-6 km).

Results from the 0-D model for individual points in the free troposphere yield a collection of ozone production and loss rates. The resulting mean diurnal cycles of ozone production and loss are shown in Figure 5. To obtain regional 24-hour average ozone production and loss rates, we first binned the data into 1-km altitude bins. Within each altitude bin we divided the data into 2-hour intervals and took the mean of each time interval. The means of each 2-hour interval, with morning/evening folding used to compensate for lack of early morning measurements and with 8 hours of darkness assumed, were averaged to obtain the regional 24-hour mean vertical profiles of ozone production and loss between 2.25-6 km shown in Figure 6. Integrating over the depth of the 2.25-6 km free troposphere column, we obtain regional ozone column production and loss rates of 11 × 10^{10} molecules cm^{-2} s^{-1} and 14 × 10^{10} molecules cm^{-2} s^{-1}, respectively.

The ozone production rate is particularly sensitive to the NO mixing ratio, while the ozone loss rate is relatively insensitive to it [*Fishman et al.*, 1979]. Any systematic offset in the NO measurement is believed to be less than 3 pptv [*Sandholm et al.*, 1994]. We conducted an uncertainty anal-

ysis on the ozone production rate by repeating the ensemble of point model calculations using measured concentrations of NO ± 3pptv. The resulting range in ozone production for the 2.25-6 km column is 8 -14 × 10^{10} molecules cm^{-2} s^{-1}.

The 0-D modeling approach that we used for the free troposphere is inadequate in the boundary layer because of the importance of isoprene and its decomposition products in modifying ozone production and loss. Because the lifetime of isoprene is only a few hours while some of its oxidation intermediates have longer lifetimes, local steady state between isoprene concentrations sampled from the aircraft and isoprene oxidation products cannot be assumed. A more realistic approach, which we adopt here, uses a diel 1-D model for the boundary layer with isoprene emission as a boundary condition. The presence of isoprene and its oxidation products result in an increase in peroxy radical concentrations and hence in ozone production.

A full description of the 1-D boundary layer model is given by *Fan et al.* [1994]. The model input is obtained from ground-based and aircraft measurements made during spirals over an instrumented tower at Schefferville, Quebec (Figure 1) on August 7, 1990. These measurements were typical of the regional background air as previously defined. The 24-hour average isoprene emission flux is specified at 6.1 × 10^{10} molecules cm^{-2}s^{-1} to match the isoprene concentrations observed in the aircraft spirals. The resulting 24-hour mean ozone production rate for the boundary layer column (0-2.25 km) is 9 × 10^{10} molecules cm^{-2}s^{-1} with an estimated uncertainty based on NO ± 3 pptv of 7 - 11 × 10^{10} molecules cm^{-2} s^{-1}. The 24-hour mean ozone loss rate in the column is also approximately 9 × 10^{10} molecules cm^{-2} s^{-1}. Summing the free troposphere and boundary layer columns yields 24-hour mean regional ozone production and loss rates for the 0-6 km column of 20 (15-25) × 10^{10} molecules cm^{-2} s^{-1}, and 23 × 10^{10} molecules cm^{-2} s^{-1}, respectively. Since our primary intent is to compare the magnitude of source terms, no attempt is made to calculate uncertainties in loss rates.

Advection of Midlatitude Pollution Ozone

To estimate the contribution from the long-range transport of urban/industrial midlatitude pollution ozone to the ozone budget at remote high northern latitudes, we assume that the chemical signatures of the anthropogenic plumes sampled during the expedition are representative of pollution advected to high northern latitudes. Following *Wofsy et al.* [1994], we identify anthropogenic plumes in the ABLE 3B data set by enhancements in C_2Cl_4 mixing ratios above background levels simultaneously with enhancements in other halocarbons, CO, C_2H_2, and NO_y. C_2Cl_4 is a particularly good indicator of anthropogenic pollution because emission of C_2Cl_4 occurs primarily in urban and industrial regions during its use as a dry cleaning and metal degreasing solvent and because it has no natural sources. To obtain a characteristic enhancement of $\Delta O_3/\Delta C_2Cl_4$ for midlatitude pollution (Δ gives the enhancement in a pollution plume above the local background level), we multiply the mean an-

thropogenic pollution enhancement ratio $\Delta CO/\Delta C_2Cl_4$ = 3800 molecules/molecule observed in ABLE 3B [*Wofsy et al.*, 1994] by the mean $\Delta O_3/\Delta CO$ observed in pollution plumes. We choose not to calculate $\Delta O_3/\Delta C_2Cl_4$ directly, as the ΔC_2Cl_4 signal above background mixing ratios can be difficult to quantify in individual plumes. $\Delta O_3/\Delta C_2Cl_4$ is then scaled by the net flux of C_2Cl_4 advected from midlatitudes and Eurasia ($\Phi_{C_2Cl_4}$) to obtain the corresponding net flux of pollution O_3 (Φ_{O_3}):

$$\Phi_{O_3} = \Phi_{C_2Cl_4}\left(\frac{\Delta O_3}{\Delta C_2Cl_4}\right) \tag{1}$$

$$= \Phi_{C_2Cl_4}\left(\frac{\Delta O_3}{\Delta CO}\right)_{mean}\left(\frac{\Delta CO}{\Delta C_2Cl_4}\right)_{mean}$$

The above expression is based on a simple model viewing the high northern latitudes as a well-mixed box. Air flowing from mid-latitudes into this box contains background mixing ratios of compounds A and B (A_b, B_b) plus pollution enhancements (ΔA, ΔB). Air flowing out of the box contains background mixing ratios (A_b, B_b). We assume that background concentrations at mid latitudes and high latitudes are the same. Thus the net flux of A into the high latitudes box is given by: $\Phi_A = F_{in}(A_b + \Delta A) - F_{out}A_b = F\Delta A$. Here F_{in} and F_{out} are the air mass fluxes in and out of the box, respectively ($F_{in}=F_{out}=F$). Similarly for B: $\Phi_B = F \Delta B$. This implies: $\Phi_B = \Phi_A (\Delta B/\Delta A)$. We can then obtain equation (1) by setting $B = O_3$ and $A = C_2Cl_4$.

The net flux of C_2Cl_4, $\Phi_{C_2Cl_4}$ (molecules cm^{-2} s^{-1}) from mid-latitudes and Eurasia to the remote high northern latitudes region is estimated from the ABLE 3B data by using a mass balance approach for the 0-6 km column adapted from *Wofsy et al.*, [1994]:

$$\Phi_{C_2Cl_4} = \left(k[C_2Cl_4][OH] + \frac{\partial[C_2Cl_4]}{\partial t}\right)\Delta z \tag{2}$$

The first term on the right of equation (2) represents the photochemical loss of C_2Cl_4 in the region. $k = 1.3 \times 10^{-13}$ molecules cm^{-3} s^{-1} is the rate constant for the reaction of OH with C_2Cl_4 at 280 K, the mean temperature of the 0-6 km column. $[OH] = 1 \times 10^6$ molecules cm^{-3} is the 24 hour mean concentration calculated in the 0-D model for the region. $[C_2Cl_4] = 12$ ppt is the mean background concentration measured in ABLE 3B (this concentration is independent of altitude, as shown in Figure 3). A mean 0-6 km column air density of 1.9×10^{19} molecules cm^{-3} is used to convert from pptv giving a photochemical loss rate of 29.4 molecules cm^{-3} s^{-1}. The second term, $\partial[C_2Cl_4]/\partial t = -4.4$ molecules cm^{-3} s^{-1}, is the rate of change in concentration in the ABLE 3B region during the July-August observation period [*Wofsy et al.*, 1994]; it amounts to less than 15% of the first term. Multiplying by the depth of the 0-6 km column (Δz), we obtain $\Phi_{C_2Cl_4} = 1.5 \times 10^7$ molecules cm^{-2}s^{-1}.

Pollution plumes used to derive the $\Delta O_3/\Delta CO$ enhancement ratio for equation (1) are required to satisfy three cri-
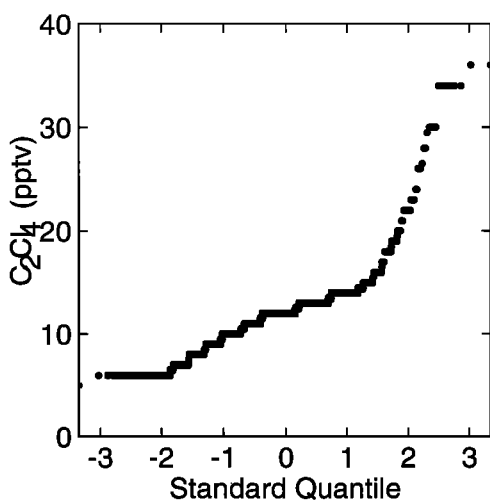
Figure 7. Probability distribution function of C_2Cl_4 concentrations in ABLE 3B.

teria. First, they must show a clear influence from combustion, evidenced by enhancements in CO and acetylene. Second, they must be clearly anthropogenic, evidenced by C_2Cl_4 enhancements of at least 2.5 pptv or CH_3CCl_3 enhancements of at least 5 pptv above local background levels. As shown by the pdf of C_2Cl_4 in Figure 7, a 2.5 pptv enhancement above background is already indicative of a pollution plume. Third, the NO_x/NO_y ratio in the plumes must be less than 0.2, indicating that the primary ozone production potential of the plume has been nearly exhausted [*Trainer et al.,* 1993; *Chin et al.,* 1994]. Table 1 is a compilation of enhancement ratios for the anthropogenic pollution plumes in ABLE 3B meeting the three above criteria. The average enhancement ratio is: $\Delta O_3/\Delta CO = 0.5 \pm 0.5$ molecules/molecule.

Figure 8 shows sample plots from a spiral on mission 6. We diagnose the plume at 5 km as anthropogenic due to strong enhancements over local background concentrations in CO, C_2H_2, NO_y, C_2Cl_4 and CH_3CCl_3. However, we diagnose a biomass wildfire origin for the plume at 3 km due to strong enhancements in CO, C_2H_2, and NO_y, but without enhancements in either C_2Cl_4 or CH_3CCl_3. This determination is consistent with back trajectories [*Shipham et al.,* 1994].

Using equation (1) and values calculated as described above for $\Phi_{C_2Cl_4}$, $\Delta O_3/\Delta CO$, and $\Delta CO/\Delta C_2Cl_4$, we obtain an estimate for the net influx of urban/industrial ozone to the remote high northern latitudes of $\Phi_{O_3} = 3 \times 10^{10}$ molecules $cm^{-2}s^{-1}$ within a range of 1 - 5 $\times 10^{10}$ molecules $cm^{-2}s^{-1}$.

Biomass Burning Plumes

Plumes which meet the combustion and aged criteria, but which show no enhancement in halocarbon concentrations are attributed to biomass wildfires. We scale up from the mean enhancement ratio ($\Delta O_3/\Delta CO$) observed within aged wildfire plumes to the net contribution, B_{O3}, of these plumes to the regional ozone budget, using:

$$B_{O_3} = E_{CO}\left(\frac{\Delta O_3}{\Delta CO}\right)_{mean} \tag{3}$$

E_{CO} is the emission rate of CO from wildfires north of 45°N during July and August of 1990. A global database for biomass burning (J. A. Logan and R. Yevich, manuscript in preparation, 1995), gives an estimate of 260 Tg for the mean quantity of biomass annually burned north of 45°N during the 1980s. We assume a 50% carbon content for biomass fuel [*Stocks,* 1991] and a mean emission ratio CO/C = 9.5% for biomass fires [*Ward and Hardy,* 1991]. Statistics available for Canada indicate that burning in July and August of 1990 represented 31% of the total mean area annually burned during the 1980s [*Higgins and Ramsey,* 1992]. We thus estimate $E_{CO} = 5 \times 10^{10}$ molecules $cm^{-2}s^{-1}$ for the circumpolar cap north of 45°N during July and August of 1990.

Table 2 provides enhancement ratios of aged biomass wildfire plumes sampled in ABLE 3B. The mean enhancement of the nine plumes is $\Delta O_3/\Delta CO = 0.1 \pm 0.2$ molecules/molecule. $\Delta O_3/\Delta CO$ enhancements in the aged wildfire plumes are approximately one-fifth the $\Delta O_3/\Delta CO = 0.5 \pm 0.5$ molecules/molecule observed in aged pollution plumes. This is likely due to the lower NO_x/CO emission ratio in biomass fires than in urban/industrial pollution [*Jacob et al.,* 1992a]. Similar $\Delta O_3/\Delta CO$ enhancement ratios have been previously reported for biomass burning plumes sampled in

Table 1. Concentration Enhancements (Δ) in Aged Anthropogenic Pollution Plumes

Mission	Plume Altitude, km	ΔO_3, ppbv	ΔCO, ppbv	ΔNO_x, pptv	ΔNO_y, pptv	$\Delta NO_x/\Delta NO_y$	$\Delta O_3/\Delta CO$
6	5.0	16	150	U	2100	U	0.11
10	3.3	21	40	30	150	0.2	0.53
16	3.2	4	24	10	200	0.05	0.17
16	4.5	13	10	28	250	0.11	1.3
22	3.0	12	60	40	900	0.04	0.2
							0.5 ± 0.5 (mean)

U, undetectable.
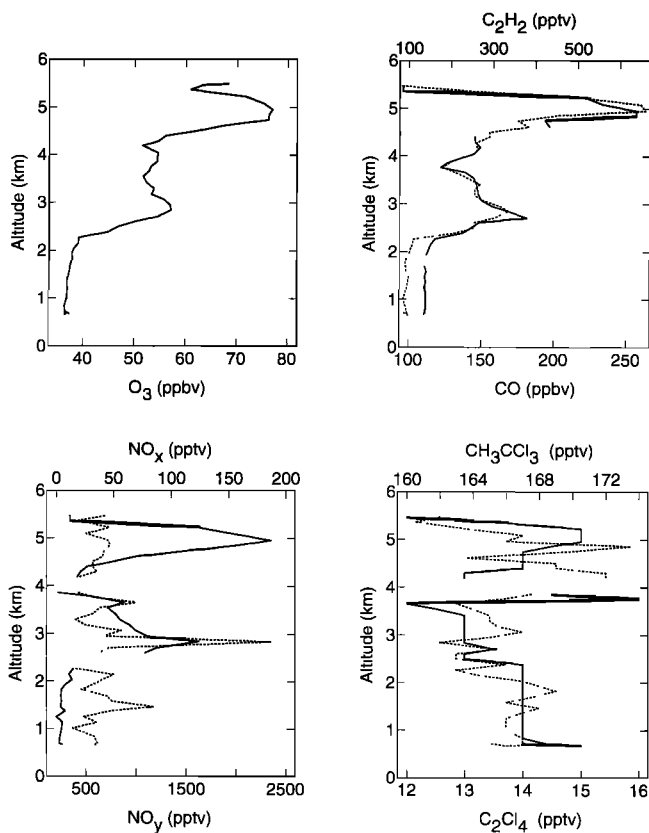
Figure 8. Vertical spiral from mission 6 on July 21, 1990 at 56°N, 105°W. Concentrations of O_3, CO, NO_y and C_2Cl_4 are indicated with solid lines; concentrations of C_2H_2, NO_x and CH_3CCl_3 are indicated with dotted lines. A pollution plume is diagnosed at 5 km. A biomass burning plume is diagnosed at 3 km.

other regions of the world [*Lelieveld et al.*, 1995], while higher values, up to 0.9, have been reported for biomass burning plumes in the tropics which have aged several days in the free troposphere [*Andreae et al.*, 1994, *Mauzerall et al.*, 1995].

We thus estimate B_{O3} = 0.5 × 10^{10} molecules cm^{-2}s^{-1} as the net contribution of biomass wildfire plumes to the regional ozone budget north of 45°N during ABLE 3B. Accounting only for the uncertainty in the enhancement ratio we obtain a range of 0 - 1.5 × 10^{10} molecules cm^{-2} s^{-1}. Ozone production within wildfire plumes thus appears to be a relatively negligible ozone source. As pointed out by *Fan et al.* [1994] and *Singh et al.* [1994], dispersion of PAN produced in fire plumes may provide a major source for the background NO_x observed in ABLE 3B. Biomass fires may thus have a major effect on regional ozone, not through ozone production in the fire plumes themselves, but rather through enhancement of background NO_x mixing ratios.

Deposition

We estimate the ozone deposition flux north of 45°N based on a map of surface types with 1° × 1° resolution from *Matthews* [1985], and a mean summertime deposition velocity for each surface type as given by *Jacob et al.* [1992b]. The deposition velocity is referenced to 200 m altitude, where data from both ABLE 3A and ABLE 3B indicate a relatively homogeneous ozone concentration of about 25 ppbv [*Browell et al.*, 1992, 1994]. Table 3 indicates the areal extent and ozone deposition velocity characteristic of each major surface type found north of 45°N. Using an ozone concentration of 25 ppbv at 200 m, we estimate a regional ozone deposition flux of 9.4 × 10^{10} molecules cm^{-2} s^{-1}. We estimate uncertainty in this value at less than 50%.

Stratospheric Influx

The final term in our ozone budget is the downward flux across the 6-km altitude level representing the transport of ozone from the stratosphere and also the effect of net photochemical production in the upper troposphere. The upper troposphere is in general a net photochemical source of ozone [*Liu et al.*, 1980], but this source cannot be quantified for high northern latitudes in summer because no observa-

Table 2. Concentration Enhancements (Δ) in Aged Biomass Wildfire Plumes

Mission	Plume Altitude, km	ΔO_3, ppbv	ΔCO, ppbv	ΔNO_x, pptv	ΔNO_y, pptv	$\Delta NO_x/\Delta NO_y$	$\Delta O_3/\Delta CO$
4	1.9	U	120	110	1200	0.092	U
6	2.8	12	65	250	1500	0.17	0.185
8	3.6	U	120	U	300	U	U
9	3.0	U	70	20	650	0.031	U
11	3.8	U	85	U	1200	U	U
11	4.7	6	260	20	5000	0.004	0.023
13	2.7	U	20	40	270	0.15	U
13	4.4	19	60	20	470	0.15	0.317
19	4.7	21	32	U	200	U	0.66
							0.1 ± 0.2 (mean)

U, undetectable. For averaging, considered equal to zero.

Table 3. Areal Extent and Ozone Deposition Velocities for Surface Types North of 45°N in Summer

Surface Type	% Total Area[a]	Deposition Velocity,[b] cm s^{-1}
Tundra	9.6	0.20
Deciduous Forest	12.1	0.26
Evergreen Forest	14.1	0.23
Shrub	2.5	0.31
Grassland	6.4	0.42
Cultivated	5.5	0.43
Ocean	45.6	0.025
Ice	4.2	0.025

[a] Fraction of the total area north of 45°N contributed by each land type. From *Matthews* [1985].

[b] *Jacob et al.* [1992b]; referenced to 200-m altitude.

tions of NO$_x$ are available. Literature estimates are, however, available for the cross tropopause flux of ozone. *Holton* [1990] calculates a mass flux of air north of 23°N downwards across the 100 mbar surface of 19.8×10^8 kg s^{-1} in summer. Multiplying this value by the mean 100 mbar ozone mixing ratio at the Goose Bay and Churchill sondes stations in July and August of 1990 (825 ± 175 ppbv) [*Environment Canada*, 1990] yields a cross-tropopause ozone flux north of 23°N of 2.2×10^{10} molecules cm^{-2} s^{-1} If we assume that all the influx occurs north of 45°N, we obtain 4.6

$\times 10^{10}$ molecules cm^{-2} s^{-1}. *Levy et al.* [1985] calculate a mean annual cross-tropopause flux of approximately 5×10^{10} molecules cm^{-2} s^{-1} ozone in the northern hemisphere. At upper latitudes the exchange should be larger than average, while in summer it should be smaller than average [*Holton*, 1990]. A recent estimate of the influx of stratospheric ozone to the troposphere north of 60°N in summer, based on a meteorological analysis of ABLE 3A expedition data, obtains a value of 12×10^{10} molecules cm^{-2} s^{-1} [*Smarsh*, 1994]. Thus from the literature we estimate ozone influx from the stratosphere north of 45°N during ABLE 3B to be in the range $2\text{-}12 \times 10^{10}$ molecules cm^{-2} s^{-1}. In comparison, a derivation of the ozone flux at 6 km as the residual of our best estimates for the other terms in the ozone budget yields a value of 8.9×10^{10} molecules cm^{-2} s^{-1}. Closure of our ozone budget is reasonably well achieved.

4. Discussion

Table 4 summarizes our regional ozone budget for the 0-6 km column at remote high northern latitudes in summer. The mean 0-6 km column concentration of O$_3$ is 7.3×10^{17} molecules cm^{-2}. Photochemical loss and deposition add up to an estimated total sink of 32.4×10^{10} molecules cm^{-2}s^{-1}. The resulting ozone lifetime in the 0-6 km column is 26 days. We see from Table 4 that dispersed in situ photochemical production is the largest source of ozone in the region (62%). Influx from the stratosphere / upper troposphere is of secondary importance (27%), transport of pollution ozone from midlatitudes makes a small contribution (9%), and production of ozone within forest fire plumes is a relatively

Table 4. Ozone Budget for the 0-6 km Column at Remote High Northern Latitudes in Summer

	Column Rate, 10^{10} molecules cm^{-2} s^{-1}		Fractional Contribution to Budget, %
	Average	Range	
Sources			
Dispersed in situ photochemical production	20	15 - 25	62
Net influx at 6-km altitude from upper troposphere / stratosphere	8.9	2 - 12	27
Net influx of pollution ozone from mid latitudes	3	1 - 5	9
Net ozone production in wildfire plumes	0.5	0 - 1.5	2
Total	32.4	18 - 43.5	100
Sinks			
Dispersed in situ photochemical loss	23		70
Deposition	9.4		30
Total	32.4		100

negligible term in the budget (2%). Our conclusion that in situ photochemical production is the dominant ozone source for the region is a direct result of having separated ozone photochemical production from loss.

Earlier analyses of the Arctic and Subarctic during ABLE 3A concluded that the stratosphere provided the primary source of ozone to the high latitude (>60°N) troposphere in summer [Browell et al., 1992; Gregory et al., 1992]. Jacob et al.[1992a] calculated net ozone production $(P-L)_{O_3}$ using the ABLE 3A data set and found that although regional NO_x concentrations suppressed net photochemical loss and doubled ozone lifetimes compared with a NO_x free atmosphere, $(P-L)_{O_3}$ was negative and ozone concentrations in the region were regulated primarily by input from the stratosphere and losses from net photochemistry and deposition. As can be seen from Table 4, in situ photochemical production and loss nearly cancel. However, since photochemical loss operates equally on all ozone regardless of its origin, we conclude that in situ photochemical production is in fact the largest source of ozone in the region, and hence that ozone levels are critically dependent on regional background NO_x mixing ratios [Fan et al., 1994].

Ozone concentrations at high northern latitudes, both in ABLE 3B (Figure 3) and elsewhere [Logan, 1985], show a trend of increasing mixing ratios with altitude which has often been interpreted as reflecting a stratospheric source but could also be explained by net production in the upper troposphere [Liu et al. 1980; Jacob et al. 1995]. To confirm that our regional budget, as summarized in Table 4, is consistent with the observed vertical profile of ozone, we conducted an illustrative 1-D photochemical model calculation for ozone in the 0-6 km column under ABLE 3B conditions. Photochemical production and loss of ozone are computed at six model grid points (0.5, 1.5, 2.5, 3.5, 4.5, 5.5 km). The concentrations of CO, long-lived hydrocarbons, acetone, and water vapor are specified as a function of altitude from the mean values observed in background air (Figure 3). Total NO_x is specified as a function of altitude as the sum of the mean background NO and the corresponding mean value of NO_2 computed from the steady state model. Vertical transport is parameterized with an eddy diffusion coefficient $K_z = 1 \times 10^5 \, cm^2 \, s^{-1}$[Liu et al., 1984]. An upper boundary condition of 75 ppbv ozone at 6.5 km is adopted. An ozone deposition velocity of 0.15 cm s^{-1} is used (the regional average of values in Table 3). Photolysis rate constants are calculated for clear-sky conditions as described previously. The model is integrated to a diel steady state defined by the reproducibility of ozone concentrations over the 24-hour solar cycle. To examine the influence of isoprene emissions, we conducted two simulations, one without isoprene flux, the other with a diurnally varying isoprene flux characteristic of the Schefferville forest site (24-hour average emission of 6.1 × 10^{10} molecules $cm^{-2} \, s^{-1}$). The difference in ozone concentrations between these two simulations was 3 ppbv at 0.5 km and less above. Since only 25% of the region north of 45°N is forested [Mathews, 1985] and emits isoprene at a rate similar to Schefferville forest, we plot the isoprene free simulation in Figure 9.
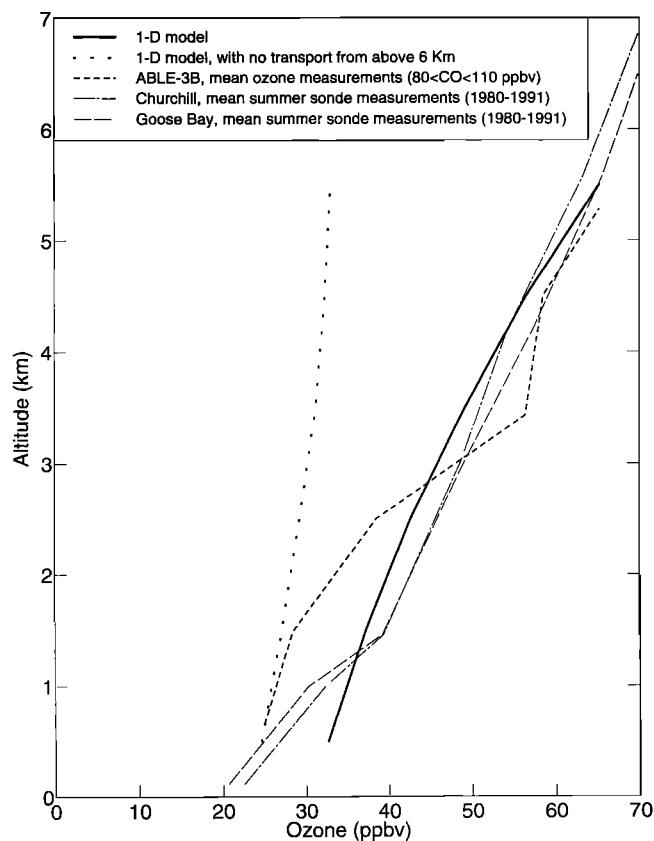
Figure 9. Vertical ozone profiles at high northern latitudes in summer including both measurements and 1-D model results.

Figure 9 shows that the 1-D model results are consistent with the observed ozone concentrations and vertical trends. Ozone production and loss in the 0-6 km column of the 1-D model are 25 × 10^{10} and 27 × 10^{10} molecules $cm^{-2} \, s^{-1}$, respectively, and ozone loss via deposition is 13 × 10^{10} molecules $cm^{-2} \, s^{-1}$. These values are 20-40% larger than those in our regional budget (Table 4). A downwards ozone flux at 6 km of 15 × 10^{10} molecules $cm^{-2} \, s^{-1}$ is needed for closure and would include contributions from pollution subsiding over the region as well as contributions from the stratosphere and from production in the upper troposphere.

Figure 9 also shows results from a 1-D sensitivity simulation with no transport of ozone across the top boundary at 6 km, i.e., with ozone concentrations determined solely by in situ photochemistry in the 0-6 km column and by deposition. When compared to ABLE 3B observations the model profile indicates that in situ photochemistry within the 0-6 km column can account for nearly 90% of ozone in the boundary layer, while above 5 km it accounts for approximately 40%. Transport from above 6-km appears necessary to reproduce the observed vertical gradient.

Our results are consistent with previous investigations of the origin of ozone at high northern latitudes based on correlations with the cosmogenic radioisotope [7]Be [Dibb et al., 1992, 1994]. These investigations documented significant stratospheric influence between 4 and 5 km altitude as indicated by elevated concentrations of [7]Be and O_3 and a de-

pressed dewpoint [*Dibb et al.*, 1992]. However, they also showed that stratospheric inputs account for at most 10-15% of O_3 at the surface in springtime and less during the rest of the year [*Dibb et al.*, 1994].

In the development of our ozone budget we have not been able to divide the natural from the anthropogenic contribution to the photochemical source term. Determination of the regional sources of NO_x is crucial in evaluating the influence of anthropogenic activities on the ozone budget at high northern latitudes; however, these sources are not well quantified. *Talbot et al.* [1994] argue that fire emissions appear to be the dominant source of reactive odd-nitrogen in the ABLE 3B region. Decomposition of PAN can account for most of the NO_x observed between the surface and 6 km in ABLE 3B, with much of the PAN believed to originate from biomass wildfires [*Singh et al.*, 1994; *Fan et al.*, 1994]. However some transport from anthropogenic mid-latitude sources is also evident in the ABLE 3B data [*Talbot et al.*, 1994; *Singh et al.*, 1994] with pollution appearing to be a major source for periodic elevation of NO_x and NO_y within the boundary layer at Schefferville [*Bakwin et al.*, 1994]. To fully characterize the anthropogenic influence on the ozone budget in remote regions, a better understanding of the sources of PAN and other long-lived reactive nitrogen compounds to these regions is needed.

Figure 9 indicates that ozone mixing ratios measured during ABLE 3B in the boundary layer were approximately 10 ppbv below the 12 year (1980-1991) July-August mean concentrations derived from ozone sonde measurements at Goose Bay and Churchill. Mixing ratios in the free troposphere were in closer agreement. The disparity in the boundary layer might reflect the fact that burning which occurred in Canada in July and August of 1990 was only 60% of the average burning which typically occurred during these two months in the 1980s [*Higgins and Ramsey*, 1992]. However, analysis of the interannual variability of tropospheric ozone concentrations at Goose Bay over the period 1970-1993 shows no correlation between years of unusually large fire areas in Canada or Alaska and years of elevated ozone concentrations [*Logan*, 1994]. Long-range transport of fire products and/or anthropogenic pollution from Asia could possibly contribute significant NO_x to the region via decomposition of PAN and other long-lived reactive nitrogen compounds. Such a contribution could obscure the influence of Canadian and Alaskan fires on ozone concentrations at these two sondes stations.

5. Summary

From data analysis and modeling using the measurements made during the ABLE 3B expedition, we find that dispersed in situ photochemical production is the largest source of ozone in the 0-6 km column at remote high northern latitudes in summer (62%). We find influx of stratospheric ozone to be of secondary importance (27%), long-range transport of pollution ozone to make a small contribution (9%), and photochemical production of ozone within biomass burning plumes to be a relatively negligible term in

the budget (2%). Illustrative 1-D model simulations indicate that within the boundary layer in situ photochemistry can account for nearly 90% of the ozone mixing ratio, while above 5 km it accounts for only about 40%. However, although photochemical production of ozone within the 0-6 km column is larger than the other source terms combined, downward transport of ozone produced in the upper troposphere or stratosphere is necessary to explain the trend of increasing ozone mixing ratio with altitude.

The high northern latitudes are both a region of particularly strong transport from the stratosphere to troposphere [*Danielsen*, 1968; *Shapiro et al.*, 1987] and an area where NO_x concentrations are typical of the remote, and much lower than the urban, northern hemisphere troposphere [*Carroll and Thompson*, 1995]. Considering that in situ photochemical production is the dominant source of tropospheric ozone even in this region, we can extrapolate with some confidence to conclude that the ozone budget on the scale of the northern hemisphere troposphere is dominated by tropospheric photochemical production and loss. A better understanding of the NO_x budget is necessary to determine the fraction of photochemical ozone production that is due to anthropogenic rather than to natural NO_x emissions.

References

Anderson, B.E., G. L. Gregory, J. D. W. Barrick, J. E. Collins, G. W. Sachse, M. C. Shipham, and C. H. Hudgins, Summertime tropospheric ozone distributions over central and eastern Canada, *J. Geophys. Res.*, 99, 1781-1792, 1994.

Andreae, M.O., B. E. Anderson, D. R. Blake, J. D. Bradshaw, J. E. Collins, G. L. Gregory, G. W. Sachse, and M. C. Shipham, Influence of plumes from biomass burning on atmospheric chemistry over the equatorial and tropical South Atlantic during CITE 3, *J. Geophys. Res.*, 99, 12,793-12,808, 1994.

Atkinson, R.A., Gas-phase tropospheric chemistry of organic compounds: A review, *Atmos. Environ.*, 24, 1-42, 1990.

Atkinson, R., D.L. Baulch, R.A. Cox Jr., R.F. Hampson Jr., J.A. Kerr, and J. Troe, Evaluated kinetic and photochemical data for atmospheric chemistry: Supplement IV, *Atmos. Environ.*, 26A, 1187-1230, 1992.

Bakwin, P.S., et. al., Reactive nitrogen oxides and ozone above a taiga woodland, *l8iik*, 1927-1936, 1994.

Barrie, L. A., Arctic air pollution: an overview of current knowledge, *Atmos. Environ.*, 20(4), 643-663, 1986.

Browell, EV., C. F. Butler, S. A. Kooi, M. A. Fenn, R. C. Harriss, and G. L. Gregory, Large-scale variability of ozone and aerosols in the summertime Arctic and sub-Arctic troposphere, *J. Geophys. Res.*, 97, 16,433-16,450, 1992.

Browell, E.V., M. A. Fenn, C. F. Butler, W. B. Grant, R. C. Harriss, and M. C. Shipham, Ozone and aerosol distributions in the sum-

mertime troposphere over Canada, *J. Geophys. Res., 99,* 1739-1756, 1994.

Carroll, M.A., and A.M. Thompson, NO_x in the non-urban troposphere, in *Advances in Physical Chemistry,* edited by J. Barker, World Sci., River Edge, N.J., in press, 1995.

Chameides, W. L., and A. Tan, The two dimensional diagnostic model for tropospheric OH: An uncertainty analysis, *J Geophys. Res., 86,* 5209-5223, 1981.

Chameides, W.L., D. D. Davis, G. L. Gregory, G. Sachse, and A. L. Torres, Ozone precursors and ozone photochemistry over eastern North Pacific during the spring of 1984 based on the NASA GTE/CITE 1 airborne observations, *J. Geophys. Res, 94,* 9799-9808, 1989.

Chameides, W.L., et. al., Observed and model-calculated NO_2/NO ratios during the NASA GTE/CITE 2 field study, *J. Geophys. Res, 95,* 10,235-10,247, 1990.

Chin, M., D. J. Jacob, J. W. Munger, D. D. Parrish, and B. G. Doddridge, Relationship of ozone and carbon monoxide over North America and its implication for ozone production and transport, *J Geophys. Res., 99,* 14,565-14,573, 1994.

Crawford, J., et al., A photostationary state analysis of the NO_2/NO system based on airborne observations from the western and central North Pacific, *J. Geophys. Res.,* in press, 1995.

Danielson, E.F., Stratospheric-tropospheric exchange based on radioactivity, ozone and potential vorticity, *J Atmos. Sci., 25,* 502-518, 1968.

DeMore, W.B., S. P. Sander, D. M. Golden, M. J. Molina, R. F. Hampson, C. E. Kolb, M. J. Kurylo, C. J. Howard, and A. R. Ravishankara, Chemical kinetics and photochemical data for use in stratospheric modeling, *JPL publ., 92-20,* 1992.

Dibb, J.E., R.W. Talbot, and G.L. Gregory, Beryllium 7 and lead 210 in the western hemisphere arctic atmosphere: Observations from three recent aircraft-based sampling programs, *J. Geophys. Res., 97,* 16,709-16,715, 1992.

Dibb, J. E., L D. Meeker, R.C. Finkel, J.R. Southon, M W. Caffee, L.A. Barrie, Estimation of stratospheric input to the arctic troposphere: [7]Be and [10]Be in aerosols at Alert, Canada, *J. Geophys. Res., 99,* 12,855-12,864, 1994.

Environment Canada, Ozone data for the world, vol. 31, no 6, Atmospheric Environment Service, Halifax, N.S., 1990.

Fan, S.-M , D. J. Jacob, D. L. Mauzerall, J. D. Bradshaw, S. T. Sandholm, D. R. Blake, H. B. Singh, R. W. Talbot, G. L. Gregory, and G. W. Sachse, Photochemistry of reactive nitrogen in the subarctic troposphere in summer 1990: Observations and modeling, *J. Geophys. Res., 99,* 16,867-16,878, 1994.

Fishman, J., S. Solomon, and P.J. Crutzen, Observational and theoretical evidence in support of a significant in situ photochemical source of tropospheric ozone, *Tellus, 31,* 432-446, 1979.

Fitzjarrald, D.R., and K.E. Moore, Growing season boundary layer climate and surface exchanges in a subarctic lichen woodland, *J. Geophys. Res., 99,* 1899-1917, 1994.

Gregory, G. L., B.E. Anderson, L.S. Warren, and E. V. Browell, Tropospheric ozone and aerosol observations: The Alaskan Arctic, *J. Geophys. Res., 97,* 16,451-16,471, 1992.

Harriss, R.C., et al., The Arctic Boundary Layer Expedition (ABLE 3A): July-August 1988, *J. Geophys. Res., 99,* 16383 - 16394, 1992.

Harriss, R.C., S. C. Wofsy, J. M. Hoell Jr., R. J. Bendura, J. W. Drewry, R. J. McNeal, D. Pierce, V. Rabine, and R. L. Snell, The Arctic Boundary Layer Expedition (ABLE 3B): July-August 1990, *J. Geophys. Res., 99,* 1635 -1645, 1994a.

Harriss, R.C., et al., Carbon monoxide and methane over Canada: July-August 1990, *J. Geophys. Res., 99,* 1659 -1670, 1994b.

Higgins, D.G. and G. S. Ramsey, *Canadian Forest Fire Statistics: 1988-1990,* Petawawa Natl. Forestry Inst., Forestry Canada 1992.

Holton, J. R., On the global exchange of mass between the stratosphere and troposphere, *J. Atmos. Sci., 47,* 392-395, 1990.

Intergovernmental Panel on Climate Change. *Climate Change - The IPCC Scientific Assessment,* Cambridge Univ. Press, New York, 1990.

Jacob, D.J., et al., Summertime photochemistry of the troposphere at high northern latitudes, *J. Geophys. Res., 97,* 16421-16431, 1992a.

Jacob, D. J., S.-M. Fan, S. C. Wofsy, P. A. Spiro, P. S. Bakwin, J. A. Ritter, E. V. Browell, D. R. Bagwell, and C. H. Hudgins, Deposition of ozone to tundra, *J. Geophys. Res., 97,* 16,473-16,479, 1992b.

Jacob, D.J., et al., Simulation of summertime ozone over North America, *J. Geophys. Res., 98,* 14,797-14,816, 1993.

Lacis, A.A., D. J. Wuebbles, and J. A. Logan, Radiative forcing of climate by changes in the vertical distribution of ozone, *J. Geophys. Res., 95,* 9971-9981, 1990.

Levy, H. II, J. D. Mahlman, and W. J. Moxim, Tropospheric ozone: the role of transport, *J. Geophys. Res., 90,* 3753-3772, 1985.

Lelieveld, J., P. J. Crutzen, D. J. Jacob, A. M. Thompson, Modeling biomass burning influences on tropospheric ozone, in *The Southern Africa Fire-Atmosphere Research Initiative (SAFARI). The Ecological and Atmospheric Chemical Importance of Savannah Fires in the Southern Africa and Atlantic regions,* edited by M.O. Andreae, J.G. Goldammer, J. Lindesay, and B. van Wilgen, University of the Witwaterrand Press, Johannesburg, in press, 1995.

Liu, S.C., D. Kley, M. McFarland, J. D. Mahlman, H. Levy II, On the origin of tropospheric ozone, *J. Geophys. Res., 85,* 7546-7552, 1980.

Liu, S.C., J.R. McAfee, R.J. Cicerone, Radon-222 and tropospheric vertical transport, *J. Geophys. Res., 89,* 7291-7297, 1984.

Liu, S. C., M. Trainer, F.C. Fehsenfeld, D.D. Parrish, E.J. Williams, D.W. Fahey, G. Hubler, and P.C. Murphy, Ozone production in the rural troposphere and the implications for regional and global ozone distributions, *J. Geophys. Res., 92,* 4191-4207, 1987.

Liu, S. C., et al., A study of the photochemistry and ozone budget during the Mauna Loa observatory photochemistry experiment, *J. Geophys. Res., 97,* 10,463-10,471, 1992.

Logan, J.A., M. J. Prather, S. C. Wofsy, and M. B. McElroy, Tropospheric chemistry: A global perspective, *J. Geophys. Res., 86,* 7210-7254, 1981.

Logan, J. A., Tropospheric ozone: Seasonal behavior, trends, and anthropogenic influence, *J. Geophys. Res., 90,* 10,463-10,482, 1985.

Logan, J.A., Trends in the vertical distribution of ozone: An analysis of ozonesonde data, *J. Geophys. Res., 99,* 25,553-25,585, 1994

Matthews, E., Atlas of archived vegetation, land-use and seasonal albedo data sets, NASA, Technical Memorandum 86199, Feb. 1985.

Mauzerall, D. L., J.A. Logan, D.J. Jacob, B.E. Anderson, A.S. Bachmeier, G.W. Sachse, D.R. Blake, J.D. Bradshaw, H. Fuelberg, and B.G. Heikes, Relationships between biomass burning emissions and photochemical tracers over source regions and the tropical south Atlantic - analysis of TRACE A expedition measurements, September-October 1992, paper presented at Chapman Conference on Biomass Burning and Global Change, AGU, Williamsburg, Va., 1995.

Sandholm, et al., Summertime partitioning and budget of NO_y compounds in the troposphere over Alaska and Canada: ABLE 3B, *J. Geophys. Res., 99,* 1837-1861, 1994.

Shapiro, M.A., Turbulent mixing within tropopause folds as a mechanism for the exchange of chemical constituents between the stratosphere and troposphere, *J. Atm. Sci., 37,* 994-1004, 1980.

Shapiro, M.A., T. Hampel, and A.J. Krueger, The arctic tropopause fold, *Month. Weather Rev., 115,* 444-454, 1987.

Shipham, M. C., A. S. Bachmeier, D. R. Cahoon Jr., G. L. Gregory, B. E. Anderson, and E. V. Browell, A meteorological interpretation of the Arctic Boundary Layer Experiment, ABLE 3B, flight series, *J. Geophys. Res., 99,* 1645-1657, 1994.

Singh, H.B., et al., Summertime distribution of PAN and other reactive nitrogen species in the northern high-latitude atmosphere of eastern Canada, *J. Geophys. Res., 99,* 1821-1836, 1994.

Smarsh, D. A., Meteorological investigation of ozone anomalies during the Arctic Boundary Layer Experiment (ABLE 3A), Doctoral dissertation, Ga. Inst. of Tech., Atlanta, 1994.

Staehelin, J., J. Thudium, R. Buehler, A. Volz-Thomas, and W. Graber, Trends in surface ozone concentrations at Arosa (Switzerland), *Atmos. Environ., 28(1),* 75-88, 1994.

Stocks, B. J., The extent and impact of forest fires in northern circumpolar countries, *Global Biomass Burning,* edited by Joel S. Levine, MIT Press, Cambridge, MA, 1991.

Talbot, R. W., et al., Summertime partitioning and budget of NO_y compounds in the troposphere over Alaska and Canada: ABLE 3B, *J. Geophys. Res., 99,* 1863-1886, 1994.

Trainer, M., et al., Correlation of ozone with NO_y in photochemically aged air, *J. Geophys. Res., 98,* 2917-2925, 1993.

Tuazon, E.C., and R. Atkinson, A product study of the gas-phase reaction of methyl vinyl ketone with the OH radical in the presence of NO_y, *Int. J. Chem. Kinet., 21,* 1141-1152, 1989.

Tuazon, E.C. and R. Atkinson, A product study of the gas-phase reaction of methacrolein with the OH radical in the presence of NO_x, *Int. J. Chem. Kinet., 22,* 591-602, 1990a.

Tuazon, E.C. & R. Atkinson, A product study of the gas-phase reaction of isoprene with the OH radical in the presence of NO_x, *Int. J. Chem. Kinet., 22,* 1221-1236, 1990b.

Ward, D. E. and C. C. Hardy, Smoke emissions from wildland fires, *Environ. Int., 17,* 117-134, 1991.

Wofsy, S.C., S.-M. Fan, D. R. Blake, J. D. Bradshaw, S. T. Sandholm, H. B. Singh, G. W. Sachse, and R. C. Harriss, Factors influencing atmospheric composition over Subarctic North America during summer, *J. Geophys. Res., 94,* 1887-1897, 1994.

J. D. Bradshaw, School of Earth and Atmospheric Science, Georgia Institute of Technology, Atlanta, GA 30332.

D. R. Blake, Department of Chemistry, University of California at Irvine, Irvine, CA 92717.

S. -M. Fan, D.J. Jacob, and D. L. Mauzerall, Department of Earth and Planetary Sciences and Division of Applied Science, Harvard University, Cambridge, MA 02138 (e-mail: dlm@io.harvard.edu).

G. L. Gregory and G. W. Sachse, NASA Langley Research Center, Hampton, VA 22331.